



HAL
open science

Solvents govern rheology and jamming of polymeric bead suspensions

Anh Vu Nguyen Le, Adrien Izzet, Guillaume Ovarlez, Annie Colin

► **To cite this version:**

Anh Vu Nguyen Le, Adrien Izzet, Guillaume Ovarlez, Annie Colin. Solvents govern rheology and jamming of polymeric bead suspensions. *Journal of Colloid and Interface Science*, 2023, 629, pp.438-450. 10.1016/j.jcis.2022.09.074 . hal-03601873

HAL Id: hal-03601873

<https://hal.science/hal-03601873>

Submitted on 8 Mar 2022

HAL is a multi-disciplinary open access archive for the deposit and dissemination of scientific research documents, whether they are published or not. The documents may come from teaching and research institutions in France or abroad, or from public or private research centers.

L'archive ouverte pluridisciplinaire **HAL**, est destinée au dépôt et à la diffusion de documents scientifiques de niveau recherche, publiés ou non, émanant des établissements d'enseignement et de recherche français ou étrangers, des laboratoires publics ou privés.

Solvents govern rheology and jamming of polymeric bead suspensions

Anh Vu Nguyen Le,[†] Adrien Izzet,[†] Guillaume Ovarlez,[‡] and Annie Colin^{*,†}

[†]*ESPCI Paris, PSL Research University, MIE-CBI, CNRS UMR 8231, 10, Rue Vauquelin,
F-75231 Paris Cedex 05, France.*

[‡]*Univ. Bordeaux, CNRS, Solvay, LOF, UMR 5258, F-33608 Pessac, France*

E-mail: annie.colin@espci.psl.eu

Abstract

Despite their apparent simplicity, suspensions of hard spheres in a Newtonian fluid show complex non-Newtonian behaviors and remain poorly understood. Recent works have pointed out the crucial role of interparticle contact forces in these behaviors. Here, we show that the same (polystyrene) particles, when immersed in different Newtonian solvents, show different behaviors at both the microscopic and macroscopic scales. Thanks to interparticle force measurements in each solvent together with rheological measurements, we show how the fine details of the pairwise particle interactions impact the macroscopic behavior. The rheological properties (shear thinning, shear thickening, jamming solid fraction value) of the suspensions, made up of same particles, are shown to depend on the nature of the solvent. Here, we highlight several mechanisms at the particle scale: the swelling of polymeric particles in an organic solvent, the role of colloidal repulsive forces and inertia in suspensions with a water solution, and the variation of the friction coefficient as a function of the load for particles immersed in silicone oils. Our study provides new quantitative data to test micromechanical models and simulations. It questions the interpretation of previous experimental works. Finally, it shows the need to systematically characterize the interparticle normal and tangential forces when studying a given suspension of hard spheres in a Newtonian fluid.

Introduction

Dispersions of solid particles in liquids, also called suspensions, are soft matter systems that we encounter on a daily basis.¹ Examples for these suspensions include paints, cement

pastes, cosmetics, cocoa paste, cornstarch-water mixtures. Despite their few constituents, concentrated suspensions of hard non-Brownian particles in a Newtonian fluid display very complex flow behaviors:² shear thinning,^{3–5} shear thickening,^{6–8} density inhomogeneities,^{9–11} etc. The understanding of these behaviors – simple at first glance – has remained limited until a major advance made by Boyer et al.¹². They consider a suspension of hard spheres characterized by a given sliding microscopic friction coefficient between the particles μ_p . By borrowing the concepts of dense granular flow and thanks to dimensional analysis, they show that the flow of such suspensions at a given shear rate $\dot{\gamma}$ under a confining pressure P^p , when the viscous forces at the level of the particles are higher than the inertial forces, are described by a single dimensionless number $I_v = \frac{\eta_f \dot{\gamma}}{P^p}$. I_v is the ratio of the viscous time $\frac{\eta_f}{P^p}$ over the characteristic time of the flow $\frac{1}{\dot{\gamma}}$, and η_f is the viscosity of the solvent. In this situation, the constitutive equations of the flow of the suspension are written as:

$$\phi = g_{\mu_p}(I_v), \quad (1)$$

$$\sigma = f_{\mu_p}(I_v)P^p. \quad (2)$$

With this set of constitutive equations, the viscosity of the suspension $\eta_s = \frac{\sigma}{\dot{\gamma}}$ does not directly depend on the shear rate. It only depends on the solid fraction ϕ and on the microscopic friction coefficient μ_p . It increases with the solid fraction and diverges close to the jamming point J characterized by a solid fraction ϕ_J . This jamming fraction ϕ_J strongly depends on the shape, polydispersity, and sliding friction coefficient μ_p of the particles.^{13,14} For monodisperse spheres, ϕ_J is a monotonic decreasing function of μ_p : the value of ϕ_J can range from the random close packing (RCP), $\phi_J^0 = \phi_{\text{RCP}} = 0.64$ for frictionless spheres, to the random loose packing (RLP), $\phi_J^\infty = \phi_{\text{RLP}} = 0.55$ for highly frictional spheres.

However, non-Newtonian behaviors are observed in suspension flows. In the above framework, since η_s only varies with the solid fraction or the friction coefficient, the latter must vary with the shear stress to account for such nonlinear behaviors. In systems with constant and homogeneous ϕ , it is the relation $\mu_p(\sigma)$ that tunes the rheological behavior of the suspension.

It may seem surprising that the particle friction coefficient μ_p could depend on the shear stress σ . In fact, this dependence is not straightforward: it is believed to come from the couplings between the flow and the normal force between particles, and between this normal force and the friction coefficient.

E.g., in systems where repulsive forces exist between the particles, when σ increases, the normal forces (proportional to the particle pressure P^p) exceed the repulsive forces originating from colloidal interactions. The contacts between particles then change from a lubricated state (as long as repulsive forces prevail, at a low shear rate) to a frictional state (when the repulsive force is overcome, at a higher shear stress). This transition results in an increase of the microscopic friction coefficient between the particles. This higher interparticle friction stemming from the increasing shear stress enhances the suspension viscosity (due to the decrease of ϕ_J), resulting in the phenomenon of shear-thickening.

On the opposite, when the contacts are already frictional (e.g., in systems where particle repulsion is absent or is overcome), an increasing normal force might cause a decrease in the interparticle friction coefficient. Such mechanism is at the origin of shear-thinning behaviors observed in some suspensions of polymeric beads.^{4,15}

The previous brief review shows that the theoretical framework for describing the physics and rheology of suspensions is well-established, mostly thanks to numerical simulations. Along with them, emerging experimental studies that describe quantitatively the link between rheological properties and microscopic force measurements are getting attention from several research groups.^{4,5} These works among others¹⁶ demonstrate the crucial importance of measuring the interparticle forces and the evolution of μ_p with the normal force between pairs of particles in the understanding of non-Newtonian behaviors. Nonetheless, this latter connection between particle friction and normal force remains badly known due to a lack of experimental data, and the physical mechanisms are not yet clear.

In the present paper, we study polystyrene (PS) particles immersed in air and in three different types of solvent. By using state-of-the-art technique to measure the microscopic friction coefficient in each solvent, together with rheological measurements, we show how the fine details of the pairwise particle interactions govern the rheological properties. The rheological properties (ϕ_J value, shear-thinning behavior) of suspensions made up of the same particles depend on the nature of the solvent. Here, we highlight several mechanisms at the particle scale: the swelling of polymeric particles in an organic solvent, the role of colloidal repulsive forces and inertia in suspensions with a water solution, and the variation of the friction coefficient as a function of the load for particles immersed in silicone oils. In the latter case, a soft layer created at the particle surface is shown to play a crucial role.

Materials and Methods

Materials

We study Polystyrene particles (PS) (Dynoseeds from Microbeads AS) of diameter $d = 40 \mu\text{m}$, density $\rho = 1.05$, immersed in air and in three Newtonian solvents: aqueous solution of NaI (0.48 mol.l^{-1} , $\rho = 1.05$), silicone oil from Merck ($\rho = 0.95$, viscosity $\eta_f = 19.9 \cdot 10^{-3} \text{ Pa.s}$ at 25°C) and poly(ethylene glycol-ran-propylene glycol) monobutyl ether (PEG; $\rho = 1.05$, $\eta_f = 2.33 \text{ Pa.s}$ at 25°C). Before being mixed with the liquids, the beads are washed thoroughly in a water-isopropanol mixture (5% wt) to remove surfactants and synthesis residues; the bead cleanness is recognized when they hydrophobically cream to the water surface in the form of armored bubbles. They are then dried at 60°C , bringing them back to powder form. Except for the suspensions in water, all suspensions are thoroughly degassed in a vacuum chamber before experiment.

Tuning Fork Microscope experiments

We use a Tuning Fork Microscope (TFM) to measure the forces between the particles and the friction coefficient. The device has been described at length in our previous work; in the following we summarize the main points required to consider the obtained results.¹⁷ A PS particle is glued to the end of a tungsten tip glued itself to a quartz tuning fork, which serves as our force sensor. During a typical experiment, the attached particle is immersed in a given solvent and brought into contact with another particle, fixed on the substrate, while monitoring the resonance features.

In the following we use two different devices: a large one with 75 mm long, 6.8 mm wide and 12 mm thick prongs (in the case of high forces and very viscous solvents), and a small one with 3.05 mm long, 340 μm wide and 600 μm thick prongs (in the case of low viscosity solvents). The equivalent normal (N) and tangential (T) stiffness of the devices are $k_N = 480 \text{ kN.m}^{-1}$ and $k_T = 154 \text{ kN.m}^{-1}$ for the large prong, and $k_N = 40 \text{ kN.m}^{-1}$ and $k_T = 12 \text{ kN.m}^{-1}$ for the small one. The difference in stiffness between the two modes of oscillation is due to the change in their inertia momentum. These extremely high stiffnesses of tens or hundreds of kN.m^{-1} renders the TFM very stable against mechanical perturbations, and allows full control of the tip position, even in the presence of strong repulsive and dragging forces. This corresponds to natural frequencies and to quality factors equal to $f_N = 1410 \text{ Hz}$, $Q_N = 5300$ in air, down to $Q_N = 2700$ in PEG (which is the most viscous solvent we used), $f_T = 720 \text{ Hz}$, $Q_T = 700\text{-}630$ in air and in PEG respectively for the large TFM and to $f_N = 28 \text{ kHz}$, $Q_N = 10000$, $f_T = 16.7 \text{ kHz}$, $Q_T = 2500\text{-}4000$ for the small one.

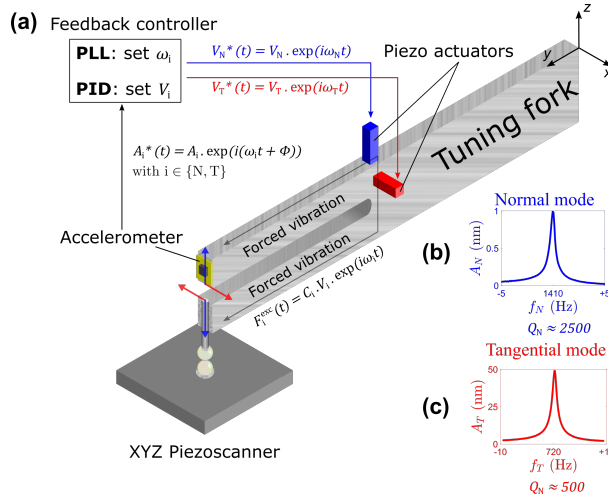


Figure 1: (a) Schematic of the Tuning Fork Microscope. A bead – glued to a quartz tuning fork – approaches another bead glued on a substrate. Both particles are immersed in a solvent. During the experiment, the tuning fork is excited at two distinct frequencies, each corresponds to a mechanical oscillation in normal ($i = N$, blue) and in tangential/shear ($i = T$, red) modes. (b) Typical resonance curve of the normal mode in air. (c) Same as (b) for the tangential mode.

The forces between the particles are the sum of conservative forces F_C and dissipative forces F_D . These latter are modeled as the sum of a viscous-like friction force and a solid friction force (F_S , independent of speed and corresponding to sliding friction for tangential motion):

$$F_{D,i} = \gamma_i v_i + F_{S,i} \frac{v_i}{\|v_i\|} \quad (3)$$

The index i refers to the unit vector \vec{e}_i along direction i (i equals N or T).

To measure simultaneously the normal and tangential force profiles between the two approaching particles, we simultaneously excite the tuning fork at two distinct resonance frequencies f_N and f_T . Owing to the very large differences in resonance frequency, the two modes are uncoupled. Both modes correspond to symmetric excitation of the prongs,

leading to negligible motion of the centre of mass and high-quality factor of the oscillator. Monitoring changes in the resonance of each mode allows us to measure respectively the normal and tangential force profiles between the two objects. A direct measurement of the conservative force field $F_{C,i}$ applied on the tuning fork is given by the shift in resonance frequency δf_i through $\nabla F_{C,i} = \vec{\nabla} F_C \cdot \vec{e}_i = -2k_i \frac{\delta f_i}{f_{o,i}}$ with i equal to N (normal component) or T (tangential component), and $f_{o,i}$ being their respective resonance frequency with no load. Monitoring the excitation voltage V^{ext} necessary to keep a constant oscillation amplitude a_0 gives us a direct measurement of the sum of all forces acting on the tuning fork as $F_i^{ext} = F_{D,i} \propto V^{ext}$; the amplitude a_0 is typically equal to 1–50 nm.

In practice, two phase-locked loops allow us to track the two resonance frequencies f_N and f_T . A proportional-integral-derivative controller (PID) keeps the oscillation amplitude a_T of the tangential mode constant, allowing a direct measurement of the frictional forces by monitoring the amplitude of the excitation voltage E_T . A fixed amplitude of the excitation voltage E_N is applied to the normal mode and dissipation is measured by monitoring the oscillation amplitude a_N . The electronic lock-in and phase-locked loops are implemented using a Nanonis from (SPECS Zurich) and a HF2LI Lock-in Amplifier (Zurich Instrument). The raw data (δf_i and V^{ext}) are corrected for thermal shifts measured when the beads are spaced apart. Then the force profiles are calculated following the above procedure. The accuracy of the measurements is estimated from the value of the forces measured when the beads are far from each other. The accuracy values depend on the device used and on the system studied. They are reported further on in the text.

In the experiments, it is important to approach the beads so that they come into contact at their apexes. Before the experiment, we put the bead glued on the tuning fork in contact with a bead glued on the bottom plate and by using a piezo scanner, we map the contact in order to find the zone which corresponds to where the apexes of the two spheres coincide. Another key parameter is the vertical location z_0 of the hard contact between the particles (where the separation between them, z , equals zero). Here, we define $z = z_0 = 0$ as the separation where the F_{DT} signal starts to rise above its noise level. This definition of z_0 is justified under the assumption that, at the contact point and in the tangential direction, the mean value of the dissipative tangential force is zero when the contact is lubricated. Note that the definition of z_0 has no impact on the estimate of the friction coefficient as a function of the normal contact force.

Rheological measurements

To study the effect of shear flow on the suspensions, we use a rheometer (TA DHR) equipped with a parallel-plate cell. The radius of the plates is equal to 20 mm and the gap between the two plates is set to 1 mm, corresponding to 25 particle diameters, so that we may neglect possible wall structuration. We glued sandpaper with a roughness of 50 μm on the plates to avoid slip at the wall. Parallel-plate geometry displays the advantage of no or low shear-induced migration,¹⁰ at least in the viscous regime. We checked that we measured a constant viscosity in time at a given shear stress and not a viscosity that drifts with time (as observed, e.g., in Couette geometries⁹). The rheometer imposes a torque T on the rotational axis and measures the angular speed of the axis Ω . A computer-controlled feedback loop on

the applied torque T can also be used to apply a constant Ω hence a constant mean shear rate without any significant fluctuation ($\frac{\delta\Omega}{\Omega} < 0.001$). From these two global quantities, the mean shear rate $\dot{\gamma}$ and the mean shear stress σ borne by the sample are calculated through the Rabinowich equation which takes into account the spatial variation of the shear rate in the parallel-plate geometry. The viscosity is extracted from the global T and Ω data using the following equations:

$$\sigma_o = \frac{2T}{\pi R^3} \quad (4)$$

$$\dot{\gamma} = \frac{\Omega R}{h} \quad (5)$$

$$\sigma = \frac{\sigma_o}{4} \left(3 + \frac{d \ln(\sigma_o)}{d \ln(\dot{\gamma})} \right) \quad (6)$$

The sample is loaded in the geometry which temperature is set to 298.15° K and controlled $\pm 0.1^\circ$ K thanks to a Peltier element. The flow curves are obtained using a shear stress-imposed flow-sweep from 100 to 0.01 Pa with 100 points per decade. The resulting shear rates are recorded each second. At the beginning of the experiments, for all experiments, we apply a shear rate step $\dot{\gamma} = 50 \text{ s}^{-1}$. This ensures that the suspension is in a shear-induced anisotropic state at the beginning of the test. We checked that the measurements thus obtained on the suspensions are in agreement with those obtained at constant imposed stress and steady measured viscosity. The procedure we use is different for suspensions in water. Indeed, due to the very low viscosity of the suspension and the inertia of the fluid, the time needed to reach equilibrium is longer in these suspensions than in other samples (typically 5 seconds for a shear rate equal to 1 s^{-1}). This induces problems with the shear stress-imposed flow-sweep and affects the viscosity measurement.¹⁸ To solve this issue, the rheometry test that is chosen for these experiments is a stress imposed step or creep test. This involves imposing a constant stress for a given period of time. After a transient comprised between 2 and 10 seconds due to the fluid inertia, the shear rate signal converges towards a plateau value before drifting after one hundred seconds. The drift might be due to a slight migration of the particles or to particles sedimentation. We report here the plateau value on the rheological curve. To compare models and experiments, we also use local rheological measurements obtained previously by Fall et al.¹⁹ using a MRI setup. In this situation, the local shear rate and the local solid fraction are measured, which allows us to deduce the local viscosity by knowing the torque applied on the axis. These measurements are not impacted by migration as the solid fraction is measured locally.

Results

In this section, we first present the contact forces measured by TFM between pairs of PS particles in air and in the three different studied solvents. We subsequently show the flow curves of the various suspensions, and we discuss the link between the different observed features and the measured contact forces.

Tuning Fork measurements

Air

In this paragraph we present the results obtained between two polystyrene beads in air. These results will serve as a basis for analysing the role of the solvents on the interactions between particles and on their friction coefficient. For this case study, we use the tuning fork with long arms. The accuracy of the measurements is characterized when the balls are very far apart and corresponds to the noise measured on V^{ext} and $\delta f_i/f_{o,i}$. The detection threshold and the accuracy are 10 nN on dissipative forces and 1 nN on conservative forces.

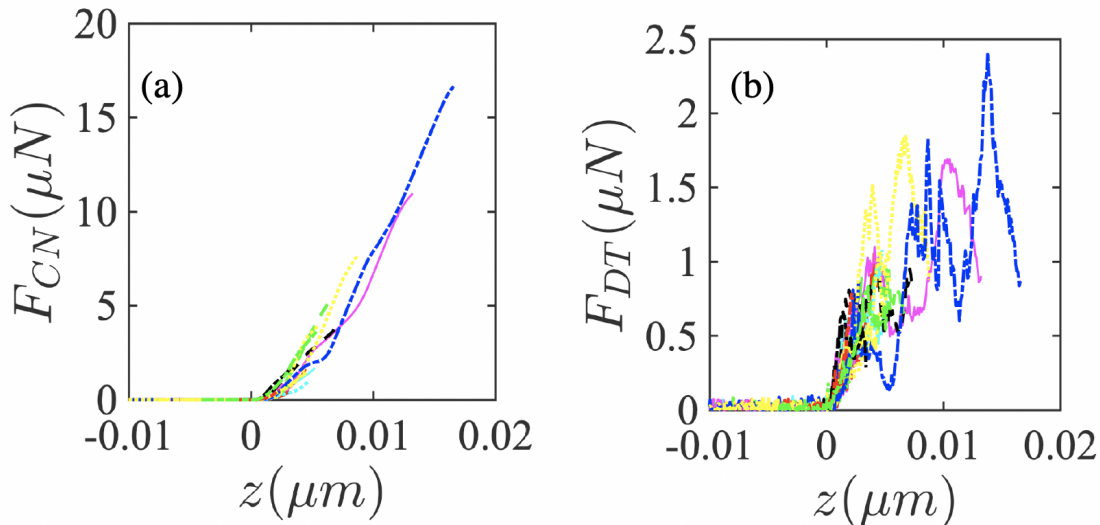


Figure 2: PS beads in air. (a) F_{CN} and (b) F_{DTI} as a function of the indentation z for 19 different measurements.

We present on figure 2 the evolution of the normal and tangential dissipative force profiles as a function of the distance z between the beads. 19 different measurements were made on the same pair of beads. The variations in the measurements reported in Fig. 2a, Fig. 2b are not surprising: they are typical of measurements at a small scale. This issue classically reported in the literature stems from the accuracy of the measurements for small forces and but also from the sensitivity of the profile to the determination of the apex positions and to the chemical heterogeneities of the surfaces.^{4,5,17} The first important feature that can be noted is that we do not observe any repulsive force between the particles in air before contact.

The same data in logarithmic scale are shown in figure 3. The conservative force varies proportionally to $z^{3/2}$. This is the expected behavior between two elastic beads of radius R in a Hertz contact, where the normal force in the elastic regime is given by $F_{CN} = ((\frac{16}{18}R)^{1/2}E^*)z^{3/2}$ with $E^* = \frac{E}{1-\nu^2}$ where E is the elastic modulus of PS and ν the Poisson ratio. The thick red dotted line in figure 3 corresponds to the evolution of F_{CN} with respect to z in a Hertz contact in the elastic regime assuming $\nu = 0.4$, $E = 3$ GPa, $R = 20$ μm , which is in quantitative agreement with the experiments.

In this regime, the sliding onset is modelled as a plastic yield failure and occurs as

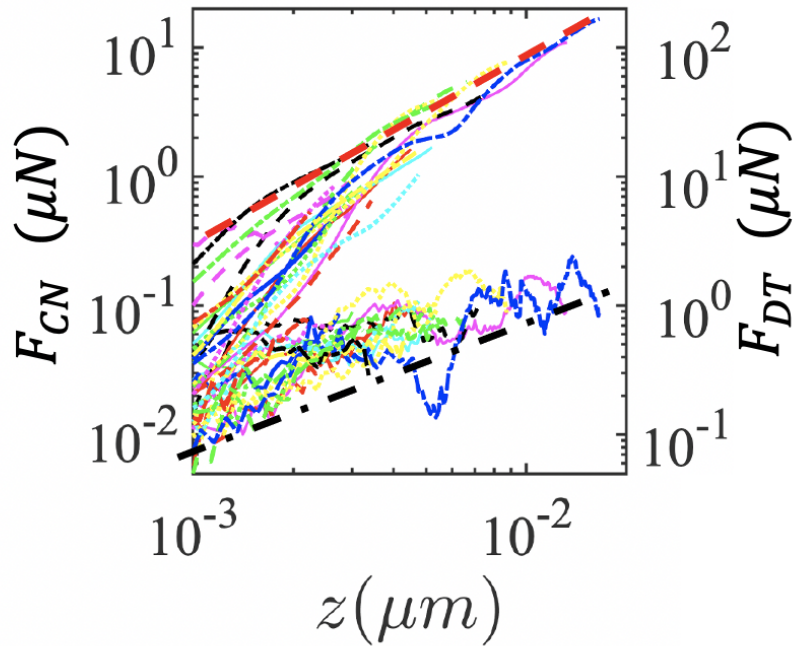


Figure 3: PS beads in air: Evolution of F_{CN} (top curves) and F_{DT} . (bottom curves) as a function of the indentation z for 19 measurements. The thick red dotted line corresponds to the Hertzian behaviour in the elastic regime: $F_{CN} = ((\frac{16}{18}R)^{1/2} \frac{E}{1-\nu^2})z^{3/2}$ with $R = 20 \mu\text{m}$, $\nu = 0.4$ and $E = 3 \text{ GPa}$. The thick black dotted line corresponds to the Hertzian behaviour in the elastic regime: $F_{DT} = \frac{16^{1/3}}{18} \pi Y_0 R z$ with $R = 20 \mu\text{m}$, $\nu = 0.4$ and $Y_0 = 2 \text{ MPa}$.

the tangential force equals $F_{DT} = Y_0 A$ where A is the contact area $A = \pi R z$ and Y_0 the yield strength. This leads to $F_{DT} = \pi Y_0 (F_{CN} (\frac{18}{16})^{1/2} \frac{R}{E^*})^{2/3} = \pi Y_0 R \frac{16^{1/3}}{18} z$. The black dotted line figure 3 corresponds to $F_{DT} = \frac{16^{1/3}}{18} \pi Y_0 R z$ with a bead radius $R = 20 \mu\text{m}$ and a yield strength $Y_0 = 2 \text{ MPa}$, which is a classical value reported in the literature for PS. It captures quantitatively the measured behavior. The quantitative agreement between a Hertzian contact model and the measurements of both F_{CN} and F_{DT} finally suggests that the PS particles are smooth elastic beads, without any significant asperity at the contact scale, characterized by an elastic modulus E of 3 GPa and a yield strength of 2 MPa, in agreement with literature values. From our measurements, the asperities involved in the particle contact – if any – would have a maximum size of order 1 nm. We already note that this observation contrasts with the asperities of order 100 nm mentioned by Lobry et al.¹⁵ to account for the suspension behavior; this will be discussed in more detail below, when commenting on the origin of shear thinning.

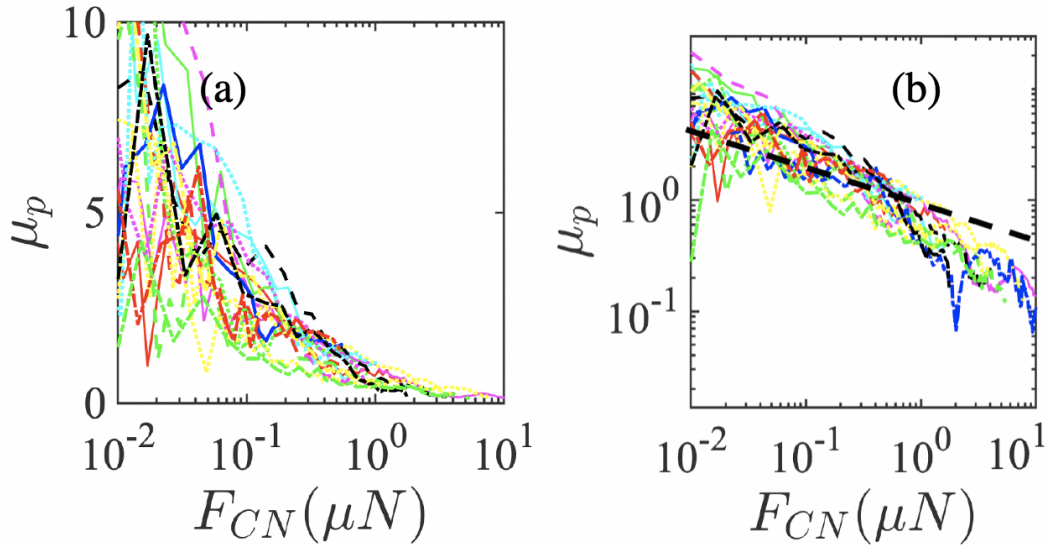


Figure 4: PS beads in air. (a) Evolution of μ_p as a function of F_{CN} . (b) Same as (a) in logarithmic scale. The thick black dotted line corresponds to a $-1/3$ slope.

It is now possible to compute a friction coefficient μ_p from the data. Figure 4 shows the evolution of μ_p as a function of the normal force. Not surprisingly, the friction coefficient $\mu_p = \frac{F_{DT}}{F_{CN}}$ variation is roughly consistent with $\mu_p = Y_0 (\frac{R}{E^*})^{2/3} F_{CN}^{-1/3}$. (see the thick black dotted line in figure 4).

Silicone Oil

Figure 5 displays the evolution of the normal conservative and the tangential dissipative force profiles as a function of the distance z between the beads. 10 different measurements have been made on two different pairs of beads. As in the case of measurements in air, we note some variability in the measurements. For this case study we used the tuning fork with

small arms. The detection threshold and the accuracy are 0.1 nN on both dissipative forces and conservative forces.

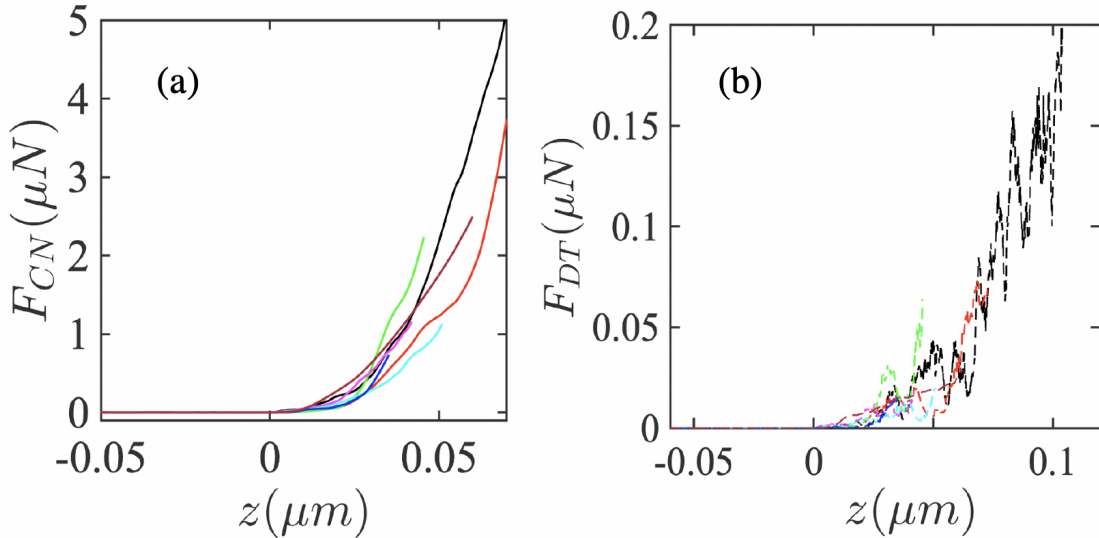


Figure 5: PS beads in silicone oil. (a) F_{CN} and (b) F_{DT} as a function of the indentation z for 10 different measurements.

As in the air situation, we do not observe any repulsive force before contact. A detailed study of the force values reveals surprisingly large discrepancies between the data obtained in air and the ones obtained in silicone oil, with two different regimes depending on indentation:

- For indentation less than 10 nm, the conservative normal forces vary as in a Hertzian contact as $z^{3/2}$ and the dissipative forces as z (see Figure 5). However, the prefactor that links F_{CN} and $z^{3/2}$ does not correspond to the value of the elastic modulus of the polymer beads measured in the previous experiments in air. It is 500 times lower, suggesting an effective elastic modulus 500 times lower than in air. We find an effective elastic modulus $E = 6$ MPa. Similarly, the prefactor that links F_{DT} and z does not match the value of the yield strength of the polymer beads measured in the previous experiments in air. The prefactor is 100 times lower, which suggests an effective yield strength 1000 times lower than in air. We find an effective yield strength $Y_0 = 0.02$ MPa.
- For indentation higher than 10 nm, the two curves become parallel and have a z -dependence close to z^3 , so that it is possible to define an exponent over one decade of z .

The crossover between these two regimes is identified at a depth $z=10$ nm. It corresponds to the indentation beyond which the contact regime is no longer elastic. These behaviours are directly reflected in the measurements of the friction coefficient. We first observe at small force a variation of μ_p as $F_{CN}^{-1/3}$ as expected in the elastic domain of a Hertzian contact, then a saturation (to a value $\simeq 0.15$) due to the entry in the plastic regime and to the fact that

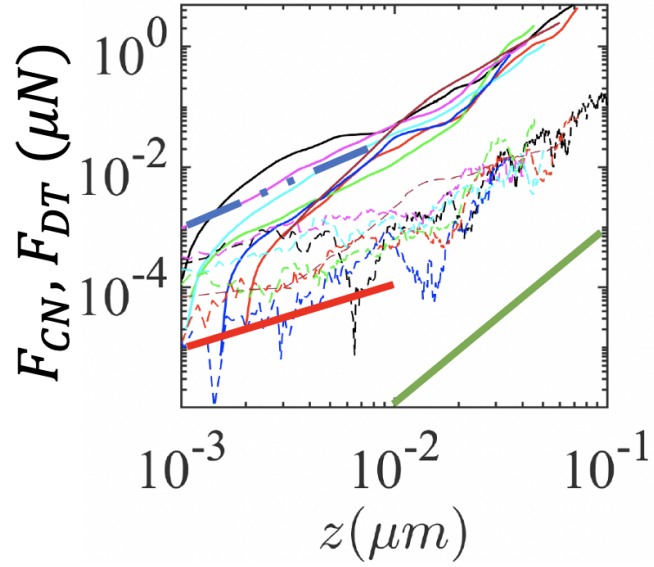


Figure 6: PS beads in silicone oil. Evolution of F_{CN} (top curves) and F_{DT} (bottom curves) as a function of the indentation z for 10 measurements. The thick blue dotted line corresponds to the Hertzian behaviour in the elastic regime: $F_{CN} = ((\frac{16}{18}R)^{1/2} \frac{E}{1-\nu^2})z^{3/2}$. The numerical application for two polystyrene spheres of radius $R = 20 \mu\text{m}$ with $\nu = 0.4$ and $E = 6 \text{ MPa}$ leads to $F_{CN} = 3 \cdot 10^4 z^{3/2}$. The red line corresponds to a slope of 1, the blue dotted one to a slope of 3/2 and the green one to a slope of 3.

the two forces F_{CN} and F_{DT} vary in the same way according to the indentation in this latter regime.

These observations are surprising. One way to explain these variations could be to invoke surface asperities. Indeed, in the presence of a rough surface with asperities, the laws linking F_{CN} and F_{DT} to indentation show the same trend as for a Hertzian contact but their prefactor is much weaker due to the size of the asperities. This description, which is the one followed in the work of Arshad et al.⁵, does not seem relevant here. Indeed, we did not notice any impact of possible asperities in the measurements with air. It is highly unlikely that asperities appear when the beads are put in the solvent.

Our analysis finally leads us to propose that the polymer is swollen by the solvent on a layer of size greater than 10 nm. This layer has a much lower elastic modulus and a much lower yield strength than polystyrene.

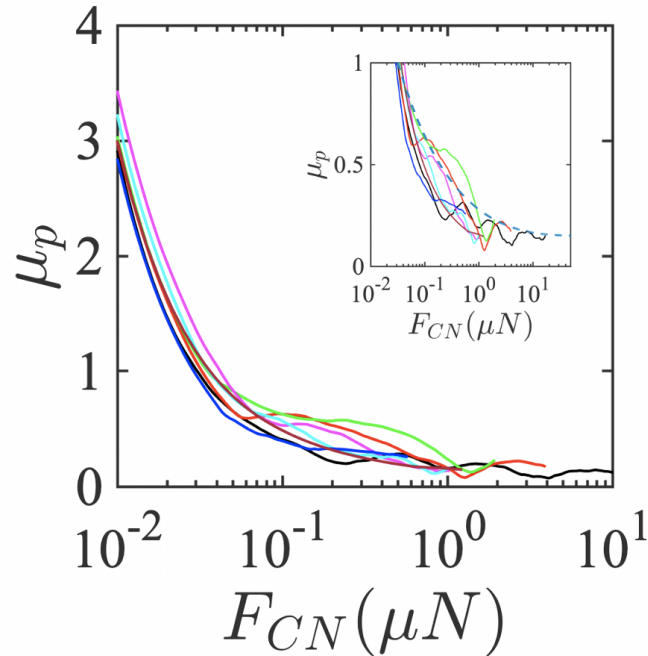


Figure 7: PS beads in silicone oil. (a) Evolution of μ_p as a function of F_{CN} . (b) Same as (a) in the zone of interest for the rheological study. The thick black dotted line in (b) corresponds to the fit used to compute the rheological properties. We use the phenomenological equation $\mu_p = 0.15 \cdot \coth(6 \cdot 10^5 \times F_{CN}^{0.4})$.

The variations of the normal and tangential forces determine the dependence of the friction coefficient on the normal force. To the best of our knowledge, there is no theoretical model predicting the z^3 evolution of the normal and dissipative forces in the domain following the elastic regime. We thus choose to adopt a phenomenological model to describe the variations of the microscopic friction coefficient. We fitted the experimental curve to the function $\mu_p = 0.15 * \coth(6 * 10^5 * F_{CN}^{0.4})$ as suggested by Maranzano and Wagner²⁰.

NaI water solution

Figure 8 displays the evolution of the profile of the normal force and of the tangential dissipative force as a function of the distance z between the beads. 15 different measurements have been made on two different pairs of beads. As in the previous measurements, we note a certain variability in the data. For this case study we used the tuning fork with small arms. The detection threshold and the accuracy is 0.1 nN on both dissipative forces and conservative forces.

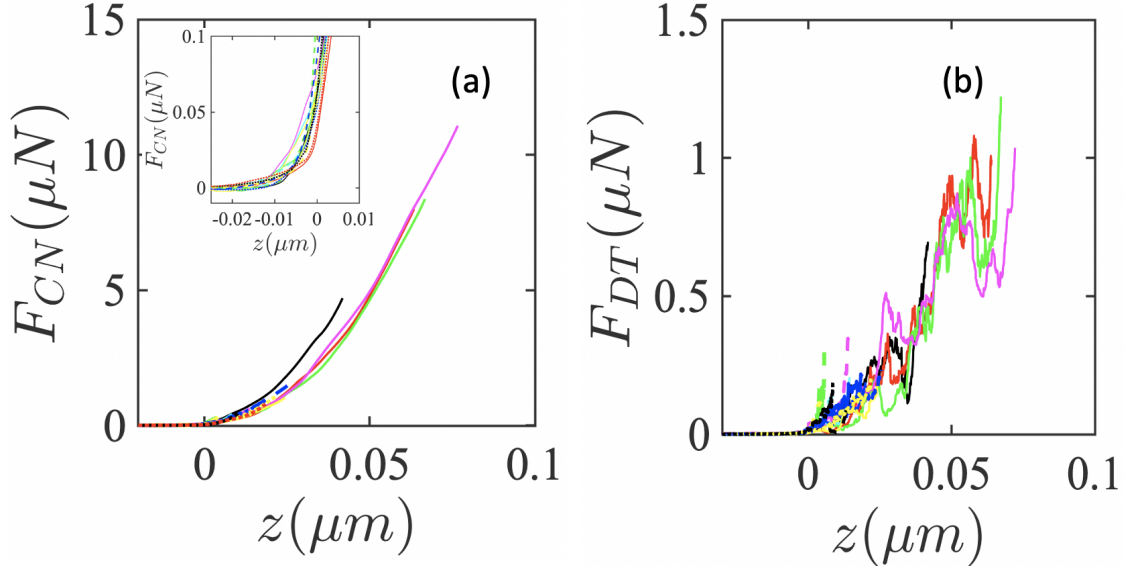


Figure 8: PS beads in water. Evolution of F_{CN} (a) and F_{DT} (b) as a function of the indentation z for 15 different measurements.

A detailed study of the force values reveals differences between the data obtained in water and the one obtained in silicone oil or in air:

- Figure 9 points out the existence of a non-zero repulsive force at contact, in contrast to what we measured in air and in silicone. We recall that contact is defined here as the emergence of a nonzero tangential dissipative force. F_{CN} does not go to zero when the indentation vanishes but rather saturates around 100 nN on average. We believe that this force is of electrostatic origin. The range of the force can be estimated to be of the order of 1 nm from figure 8 inset. The repulsive force decreases from 1 to 0.1 over $z_i = 1-4$ nm which induces a range of $\lambda = z_i/2 \ln(10)$ i.e. 0.8 nm for a force with an exponential profile. The term 2 in the above estimate comes from the fact that z refers to the distance between the two balls, both being charged. The Debye length of the 0.48 mol/l NaI solution is 0.43 nm which is consistent with the range estimated above. The existence of this electrostatic force is not surprising and may be due to the existence of sulphate anchored groups on the surface of the polystyrene during the polymerisation reaction.²¹
- F_{CN} varies as $z^{3/2}$ for indentation higher than 50 nm. The prefactor is 30 times

lower than the one measured in air but at least 17 times higher than that measured in silicone oil. Due to the presence of repulsive forces, it is not possible to deduce precisely an effective elastic modulus of the soft layer. The dissipative forces varies as z for indentation less than 50 nm and roughly as $z^{3/2}$ for indentations higher than 100 nm. (see figure 9). In this situation also, the prefactor linking F_{DT} and z in the elastic regime is 100 times higher than the one measured in silicone oil and 10 times lower than the one measured in air.

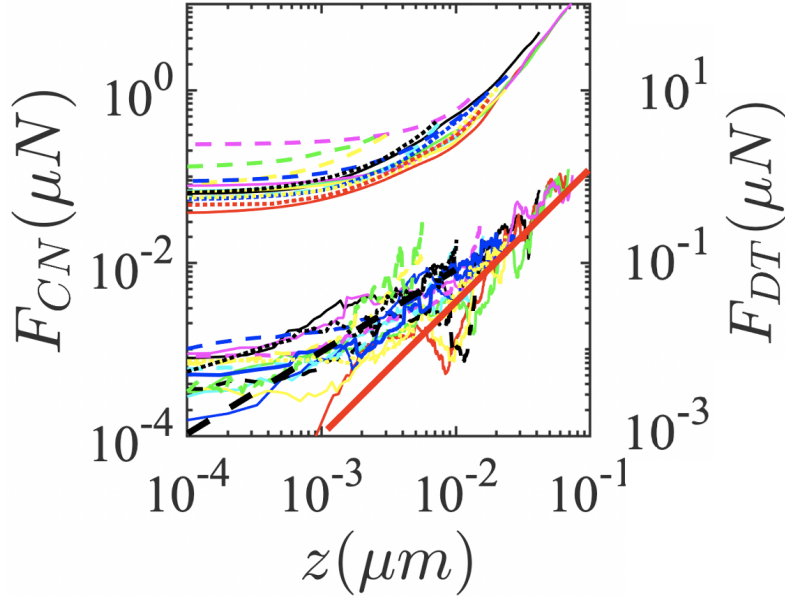


Figure 9: PS beads in water. Same data as in figure 8 in logarithmic scale. Evolution of F_{CN} (top curves) and F_{DT} (bottom curves) as a function of the indentation z for 15 measurements. The black dotted line has a slope of 1 and the red thick line a slope of $3/2$.

As in the case of silicone oil, we believe that the measured low values of the forces are due to changes in the outer layer of the particles caused by swelling of the polymer by water. Following our measurements, we assume that the size of the swollen layer is larger than 50 nm. Measurements at deeper indentations would *a priori* be necessary to probe this point. However, these measurements cause plastic changes in the particle which make a better measurement of the layer thickness tricky.

As before, variations in the measured force profiles have direct consequences on the value of the friction coefficient. The latter is only defined if there is solid contact, i.e. for normal forces greater than the force at contact ($z = 0$ nm), which is of the order of 50 nN. When the indentation is larger than 50 nm, F_{CN} and F_{DT} follow the same trend with respect to the indentation z , which means that the friction coefficient is constant. The mean value of μ_p is equal to 0.13 for F_{CN} greater than 200 nN.

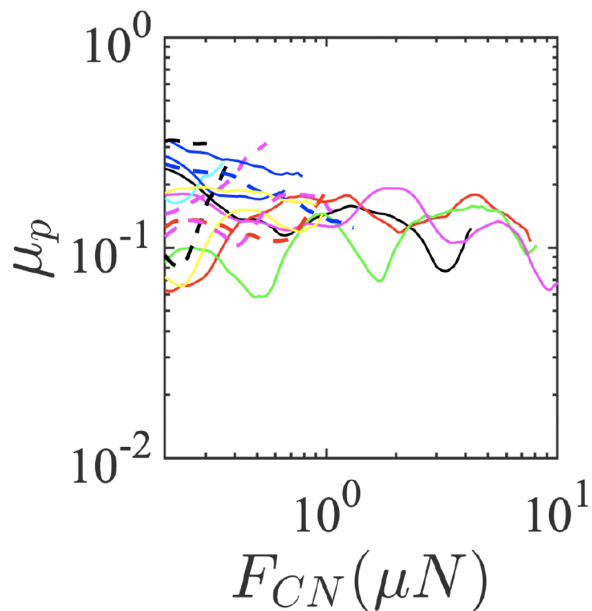


Figure 10: PS beads in water. Evolution of μ_p as a function of F_{CN} .

PEG

Figure 11 displays the evolution of the normal conservative and the tangential dissipative force profiles (see figure 12) as a function of the distance z between the beads. 19 different measurements have been made on the same pair of beads. For this case study we used the tuning fork with small arms. The accuracy is 10 nN on both dissipative forces and conservative forces. These profiles show significant differences with the previously obtained profiles.

There is a repulsive force to overcome in order to make contact. Indeed, we measure a significant conservative force for negative and dissipative indentations whereas in the same area the dissipative tangential forces are zero. The range of this force is large, of the order of 100 nm (see the zone where the conservative forces vanish on figure 11). Such a range in an organic solvent can be explained by steric forces. Our interpretation is that PEG significantly swells the PS particles, which have polymer brushes on the surface that repel each other. The indentation zone resembles what was previously measured: the conservative forces vary as $z^{3/2}$; the prefactor measured between F_{CN} and $z^{3/2}$ is 4 times weaker than in silicone and thus 2000 times weaker than in air. We interpret this as a swelling of the PS beads by PEG. A peculiarity of these profiles is that the measured dissipative forces are very weak (100 times smaller than in other solvents for the same indentation). This results in a very low value of the friction coefficient, which is found to be less than 0.05 (see figure 13).

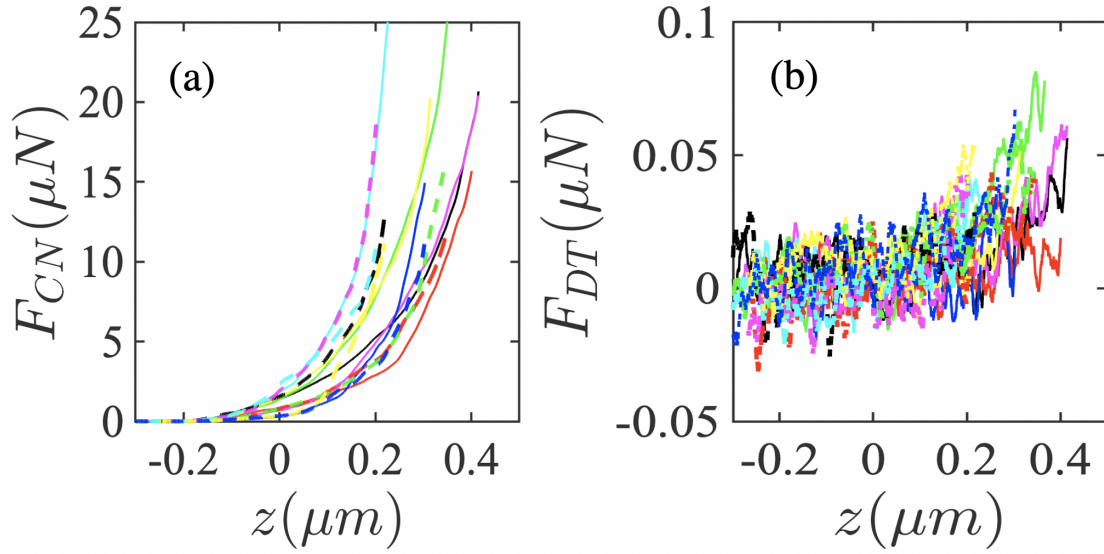


Figure 11: PS beads in PEG. Evolution of F_{CN} (a) and F_{DT} (b) as a function of the indentation z for 19 different measurements.

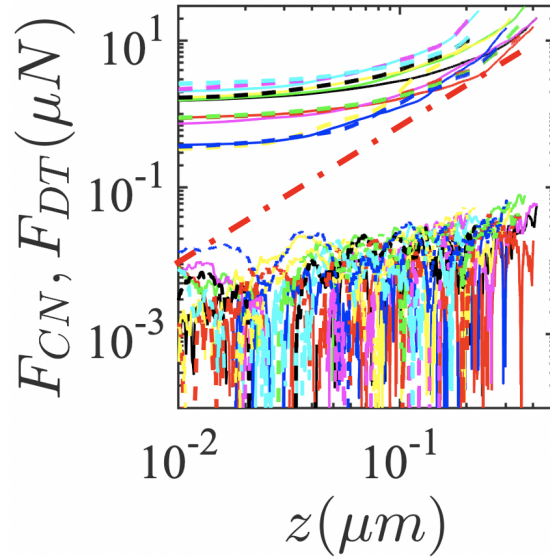


Figure 12: PS beads in PEG. Same data as in figure 11 in logarithmic scale. Evolution of F_{CN} (top curves) and F_{DT} (bottom curves) as a function of the indentation z for 19 measurements. The red dotted line has a slope of $3/2$.

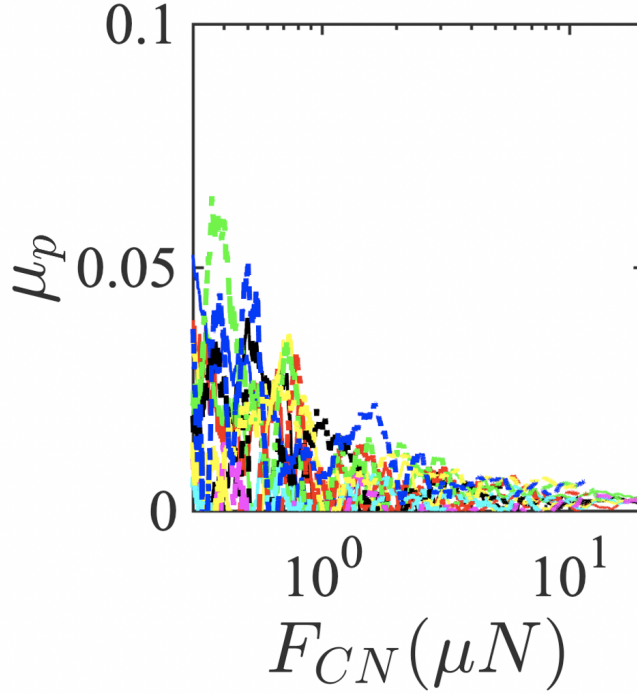


Figure 13: PS beads in PEG. Evolution of μ_p as a function of F_{CN} .

Summary and consequences

To summarize our observations, different kinds of contacts between pairs of PS beads have been found depending on the solvent. In air, the response is elastic and consistent with a Hertzian contact of smooth hard PS spheres. In the silicone oil, we found the same scaling for the contact forces as for a Hertzian contact, but for mechanical parameters corresponding to soft spheres, which suggests that the particles are covered by a soft layer of tens of nm thickness. In the NaI water solution, a repulsive force of 1 nm range, which is likely of electrostatic origin, has been evidenced. In PEG, a repulsive force of 100 nm range is observed, which points to particle swelling.

This results in different $\mu_p(F_{CN})$ profiles. For loads between 0.01 μN and 10 μN : in the water solution, the friction coefficient is roughly constant and equal to 0.12; in PEG, it is close to zero; in the silicone oil, it decreases from 2 to 0.16.

We will see in the following that these differences have huge repercussions on the rheological properties.

Rheological measurements

In the following, we report the flow curves observed in the various suspensions, and we discuss the results in relation with the TFM measurements. To make a quantitative link between the microscopic and macroscopic scales, the typical normal force between pairs of particles in the suspensions has to be estimated. Here, we use the following estimate proposed by Arshad et al.⁵ between the shear stress σ and the particle normal force F_{CN} : $F_{CN} = (6\pi R_s^2 \sigma) / 1.69$,

with R_s the particle radius; this estimate is close to that found by Singh et al.¹³ in numerical simulations.

Air

We did not perform rheological measurements for the assembly of dry particles. Indeed, flows of dry granular media have to be studied with specific pressure-imposed devices.² However, Fall et al.²² have studied the dense slow flows of granular materials made up of the same PS particles as the ones we have studied, though of 500 μm radius, in such pressure-imposed configuration. In the limit of dense slow flows, when the inertial number tends towards zero, Fall et al.²² report a solid fraction value of 0.625. This solid fraction is that of the critical state of granular materials, which is equivalent to the jamming solid fraction of the corresponding suspension² (made up of same particles, with same interparticle friction coefficient). In the Fall et al.²² experiments, the typical particle pressure is of order 100-1000 Pa, which corresponds to a normal force of $\sim 10^{-4}$ N per particle contact for the 500 μm radius particles, and would correspond to $\sim 10^{-7}$ N per particle contact for the 20 μm radius particles we study. Our contact force measurements show that, in this range of normal forces, the interparticle friction coefficient is lower than 0.1. With such low friction coefficient, the jamming solid fraction, and thus the critical state solid fraction of granular materials is expected to be of order 0.63.¹⁴ Our contact force measurements are thus in very good agreement with the critical state solid fraction measured by Fall et al.²².

Silicone oil

Figure 14a displays the evolution of the reduced viscosity $\frac{\eta}{\eta_s}$ as a function of the shear stress for suspensions prepared with polystyrene beads and silicone oil. (η_s is the viscosity of the solvent, here the silicone oil). From top to bottom the curves correspond to various solid fractions (0.55, 0.53, 0.5, 0.47, 0.45). The reduced viscosity tends to diverge at a small finite stress and then have a shear thinning behavior.

The viscosity divergence shows up as a stress plateau at low shear rate in the shear stress versus shear rate curves. This feature indicates the existence of a yield stress which is evidenced Figure 14b. The values reported are low but not zero. We measure a yield stress of 0.3 Pa for a solid fraction of 0.55. The existence of a yield stress may be understood as a consequence of the total absence of any repulsive force before the contact or of the fact that we were unable to measure very small attractive forces before the contact. The mismatch in density may also induce a gravitational stress.²³

In the following we will not consider the part of the curve close to the yield stress and we will make the hypothesis that this yield stress does not affect the rheological behavior at large shear stress. For shear stress 10 times higher than the yield stress, the suspensions display a shear thinning behavior. This behavior has already been reported by Chatté et al.⁴ and by Lobry et al.¹⁵. In both cases, the authors suggest that the variation of the friction coefficient with the load is at the origin of the shear thinning behavior. Coupling numerical simulations, rheological measurements and AFM measurements, Arshad et al.⁵ propose a quantitative description of their rheological measurements. They link the reduced viscosity to a function of the load-dependent friction coefficient. In this approach, the shear viscosity

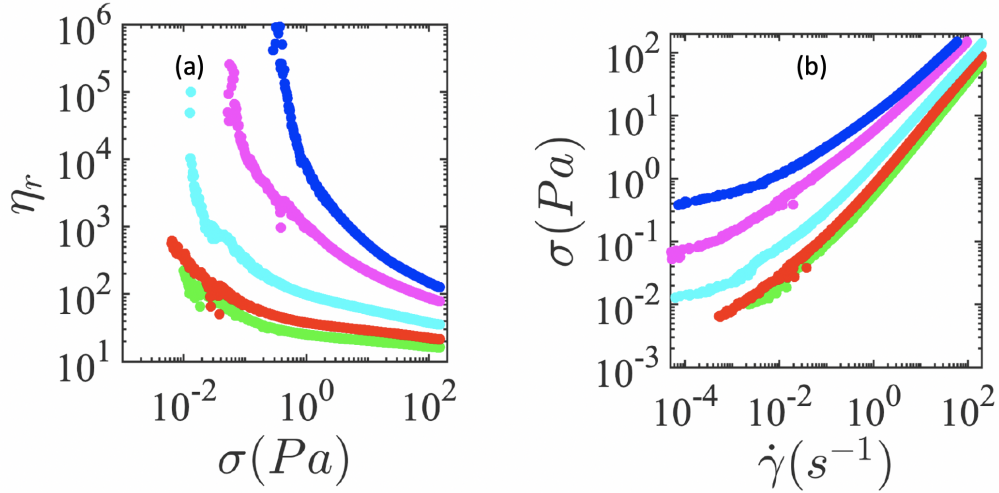


Figure 14: (a) Reduced viscosity as a function of the shear stress for a suspension of polystyrene beads in silicone oil (viscosity of the solvent 20 mPa.s⁻¹). From top to bottom the solid fraction ϕ is equal to 0.55, 0.53, 0.5, 0.47, 0.45. (b) Same measurements displayed in the shear stress versus shear rate plane.

is given by:

$$\eta_r = \frac{\alpha(\mu_p)}{\left(1 - \frac{\phi}{\phi_J(\mu_p)}\right)^2} \quad (7)$$

$$\mu_p = f(F_{CN}) \quad (8)$$

$$F_{CN} = \frac{6\pi R_s^2 \sigma}{1.69} \quad (9)$$

Lobry et al.¹⁵ propose the following phenomenological functions for $\alpha(\mu)$ and $\phi_J(\mu)$:

$$\alpha(\mu_p) = \alpha^\infty + (\alpha^0 - \alpha^\infty) \frac{\exp(-X_a \arctan \mu_p) - \exp(-\pi X_a/2)}{1 - \exp(-\pi X_a/2)} \quad (10)$$

$$\phi_J(\mu_p) = \phi_J^\infty + (\phi_J^0 - \phi_J^\infty) \frac{\exp(-X_p \arctan \mu_p) - \exp(-\pi X_p/2)}{1 - \exp(-\pi X_p/2)} \quad (11)$$

where indices ∞ and 0 denote the case of infinite and zero friction respectively.

Here we follow a similar approach. To compare our results with the simulation data, we proceed as Arshad et al.⁵ did and adjust the parameters of the previous relationships in order to find the best agreement between the rheology and the TFM experiments. Figure 15 shows the comparison between the experimental and the theoretical data for the parameters found. These parameters are different from the simulation parameters but also from the parameters deduced from the experiment by Arshad et al.⁵. This may be due to the different polydispersity of our suspensions. This value affects the value of the radius to be taken into account. We also note that we propose a fit over a larger range of solid fraction than

previously proposed which may induce a modification of the fit parameter values. Despite these slight variations, we find the main result already highlighted by Chatté et al.⁴ and then by Lobry et al.¹⁵: the decrease of the friction coefficient as a function of the normal force is a key point that accounts quantitatively for shear thinning in frictional suspensions.

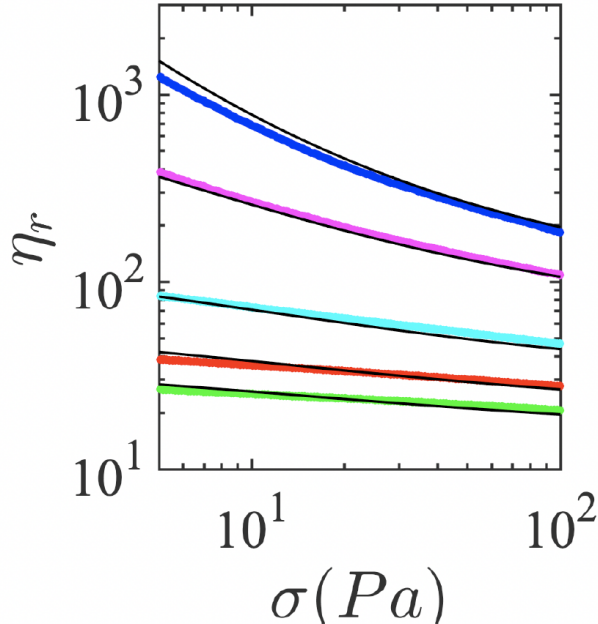


Figure 15: Reduced viscosity as a function of the shear stress for a suspension of polystyrene beads in silicone oil (viscosity of the solvent 20 mPa.s⁻¹). From top to bottom the solid fraction ϕ is equal to 0.55, 0.53, 0.5, 0.47, 0.45. The black lines correspond to the model.

The black lines are the fit curves using Equations (10) & (11) with $X_a = 1.85$, $\alpha^0 = 1$, $\alpha^\infty = 0.65$, $X_p = 2.3$, $\phi_J^\infty = 0.555$, and $\phi_J^0 = 0.63$. These values are very close to those obtained by Arshad et al.⁵ (see table 1).

To obtain these results we used the equation of the experimental curve measured with the tuning fork, which relates the microscopic friction coefficient to the normal force. This curve is fitted by a phenomenological equation:

$$\mu_p = 0.15 * \coth(6 * 10^5 * F_{CN}^{0.4}) \quad (12)$$

The model presented has many adjustable parameters. The studied suspension has a yield stress, which prevents the adjustment of the data at low stress. The determined parameters thus have an uncertainty of 0.5 to 1%.

Table 1: Comparison of the fitting parameters obtained by various studies.

Study	X_a	α^0	α^∞	X_p	ϕ_J^∞	ϕ_J^0
This study	1.85	1	0.65	2.3	0.555	0.63
⁵ exp	1.85	1	0.64	2.43	0.55	0.65
⁵ theo	1.85	1	0.64	2.43	0.56	0.7

NaI water solution

Figure 16a displays the evolution of the shear stress as a function of the shear rate for suspensions in water. From top to bottom the curves correspond to various solid fractions (0.58, 0.56). The shear stress varies linearly with the shear rate at low shear rates and then increases as the square of the shear rate above a characteristic stress, as previously reported by Madraki et al.¹⁸, Fall et al.¹⁹.

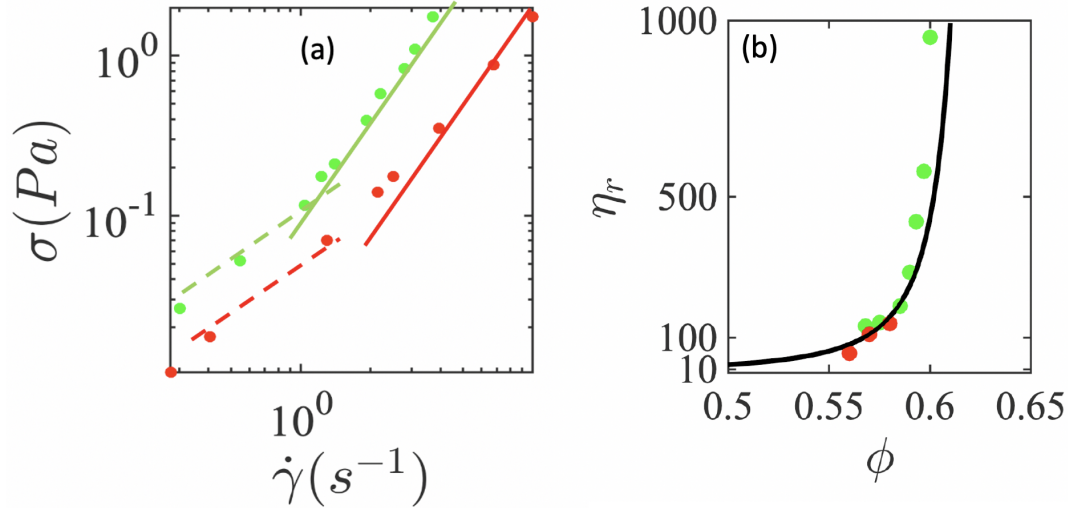


Figure 16: Aqueous solution of NaI. (a) Shear stress as a function of the shear rate. Green dots corresponds to $\phi = 0.58$ and red dots to $\phi = 0.56$. The dotted line have a slope 1 and the thick ones a slope 2. Both are guides for the eyes. (b) Reduced viscosity as a function of the solid fraction. The black line corresponds to the equation $\eta_r = \frac{1}{(1-\frac{\phi}{\phi_J})^2}$ with $\phi_J = 0.63$. The red points are measured using a rheometer, the green points are extracted from¹⁹ and deduced from NMR measurements.

In the TFM experiments, we observed that the particles are subjected to a repulsive force comprised between 30 and 300 nN. In the rheology experiments, this force can only be overcome if the applied stress is larger than a critical stress of order 5-60 Pa. In Fig. 16, the applied stress is less than this critical value, suggesting that all the particles repel each other and that the contacts are lubricated (frictionless) in the region under scrutiny.

This implies that the shear thickening observed for stresses above 0.1 Pa is not due to a change in the nature of the contacts. The change of regime corresponds to the transition to inertial regime, as suggested by Fall et al.¹⁹, and not to the appearance of frictional contacts as found in other thickening systems.⁸ Consistently, we note that the shear stress varies as the square of the shear rate, following the Bagnold law.

Let us finally comment on the value of the viscosity measured in the viscous regime where the viscosity is constant and independent of the shear rate. Figure 16 displays the viscosity values in this regime as a function of the solid fraction. The reduced viscosity varies as $\eta = \frac{1}{(1-\frac{\phi}{\phi_J})^2}$ and the value of ϕ_J is equal to 0.63 in agreement with the fact that the contacts

are frictionless in this regime. Consistently, this value is equal to the fitting parameter ϕ_J^0 obtained with the silicone oil, which corresponds to the limit of frictionless materials.

PEG

Figure 17a displays the evolution of the reduced viscosity $\frac{\eta}{\eta_s}$ as a function of the shear stress for suspensions prepared with polystyrene beads in PEG. From top to bottom the curves correspond to various solid fractions. They do not exhibit any yield stress. However, they show a strong shear thinning behavior.

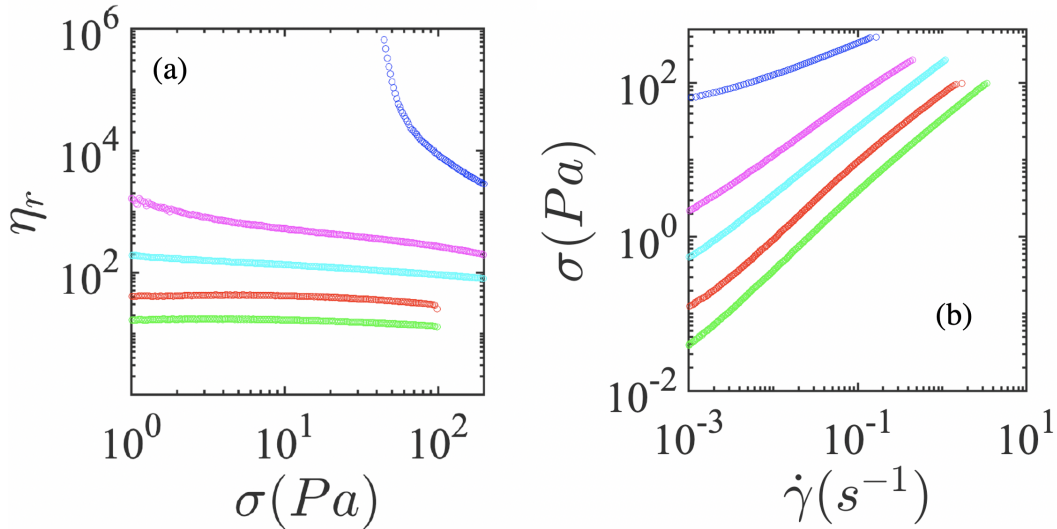


Figure 17: (a) Reduced viscosity as a function of the shear stress for a suspension of polystyrene beads in PEG (viscosity of the solvent $2.35 \text{ Pa}\cdot\text{s}^{-1}$). From top to bottom the solid fraction ϕ is equal to 0.56, 0.53, 0.51, 0.47, 0.41. (b) Same data shear stress as a function of the shear rate

As discussed in the previous section, particles in PEG are subjected to a repulsive force with a large range of interaction. The repulsive forces are very large and are not exceeded here by the hydrodynamic forces. Moreover, the measured friction coefficient is almost zero. The suspension is thus a frictionless suspension. The shear thinning behavior is based on a different principle from that acting in silicone suspensions. We believe that two mechanisms are at play here. The solvent significantly swells the beads, which on the one hand induces the long-range repulsive force that we measured. On the other hand, this swelling is accompanied by an increase in the radius of the beads. These two points lead to a redefinition of the solid fraction. The effective solid fraction is given by $\phi = \phi_o(1 + \frac{h(F_{CN})}{R})^3$, ϕ_o is the initial fraction of beads estimated over the non-swollen radius of the beads in the solvent R and defined as $\phi_o = \frac{4\pi R^3 N}{V_s + 4\pi R^3 N}$ where V_s is the solvent volume and N the number of beads. $h(F_{CN})$ is the range of the repulsive force, which goes as the inverse of $F_{CN}(z)$ in the indentation experiments (z being the indentation depth). It hence varies as a function of F_{CN} and therefore as function of σ . This leads us to use the following set of equations:

$$\eta_r = \frac{1}{\left(1 - \frac{\phi}{\phi_J}\right)^2} \quad (13)$$

$$\phi = \phi_o \left(1 + \frac{h(F_{CN})}{R}\right)^3 \quad (14)$$

$$F_{CN} = \frac{6\pi R_s^2 \sigma}{1.69} \quad (15)$$

$$h(F_{CN}) = e + z(F_{CN}) \quad (16)$$

where e is given by $R_s - R$, R_s being the radius of the swollen beads. From this set of equations and from our data, using e as a fitting parameter, we can estimate $h(F_{CN})$ and compare it to the measurements obtained using the tuning fork $z(F_{CN})$.

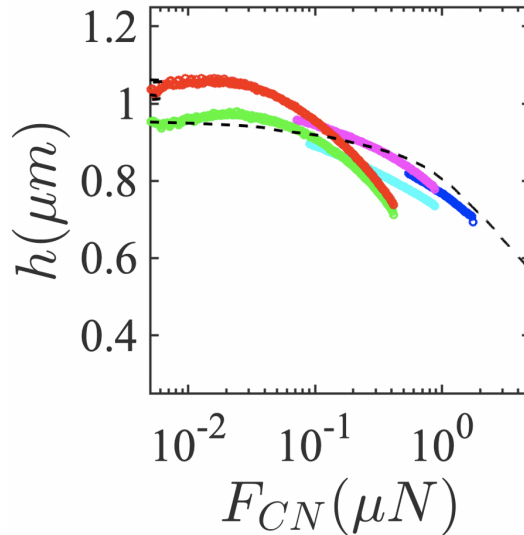


Figure 18: Evolution of h as a function of F_{CN} , the colors correspond to the different solid fractions and are the same as the ones used in figure 17 (blue: 0.56, magenta: 0.53, cyan: 0.51, red: 0.47, green: 0.41). Black dashed line is computed from the TFM measurements.

Figure 18 shows the $h(F_{CN})$ curves obtained. We note that all the data obtained for various solid fractions collapse on a single master curve. This curve is in perfect agreement with the one measured using the TFM. We use a single fitting parameter e to obtain this agreement. We estimate $e = 0.96 \mu\text{m}$. With this value, the actual volume occupied by the particles is $(1 + e/R_s)^3 = 1.08$ times higher than the volume computed based on the bulk material only. This implies in particular that the jamming volume fraction of PS in PEG, found here to be higher than 0.56 and reported to be 0.585 by Boyer et al.¹² is actually 0.63 when the effective swollen particles are considered. This value is that expected for frictionless particles, consistent with our measurement of a friction coefficient close to zero. This is discussed further below.

Discussion and Conclusion

In this work we have shown that the interactions between the solvent and the polymer beads induce strong modifications of the particles properties. In all cases (silicone oil, water solution, PEG) a soft layer is formed on the surface of the beads. The comparison of measurements made in the presence and absence of solvent allows us to assert that the contact properties are governed by this soft layer, and not by a solid layer covered by asperities as proposed by Lobry et al.¹⁵. The measurements in air are in quantitative agreement with a Hertzian contact model for smooth beads. It seems unlikely for the surface to become rough and have asperities when brought into contact with solvents. Our interpretation of this behaviour is as follows. Solvents penetrate in and swell the polystyrene. They cause a swollen layer of polymer to form. In the extreme case of PEG, the swelling is so important that it induces the formation of a polymer brush that covers the surface of the particles; this polymer brush causes long-range steric repulsion forces.

Here, we show that the particle contact is made over a small thickness which mechanical properties are weakened by the solvent, as compared to that in the bulk material. The consequences of this swelling are multiple. Some repulsive forces may appear between the particles as in the PEG situation. In all cases, the microscopic friction coefficient is lower in solvents than in air. It is even close to zero in the case of PEG.

These behaviours have important implications for the rheological properties. Particles in silicone oil have a coefficient of friction that evolves according to a Hertzian contact law before entering a plastic regime for large forces. We confirm the phenomenological analysis by Arshad et al.⁵ and show over a larger range of solid fraction and stress that Lobry et al.¹⁵ numerical simulations can account for the evolution of rheology if the dependence of the friction coefficient on the normal force is known. Nevertheless, the origin of the non-Coulomb friction law and of the resulting shear-thinning behavior, as discussed above, is not to be found in asperities, by contrast with the proposition of Lobry et al.¹⁵, but rather in the emergence of a soft layer at the particle surface. To conclude on this point, it is important to note that the mechanism proposed by the Nice group requires an important densities of asperities around the particle and a homogeneous distribution. This is not in agreement with the images presented Lobry et al.¹⁵ where the asperities are few in number and are not homogeneously distributed. The particle has large parts all smooth.

Particles in PEG have a negligible friction coefficient. This system thus behaves like a suspension without interparticle friction. These measurements are important. Indeed, in the literature, the PEG-polystyrene beads system is the reference system on which the various $\mu(I, \phi)$ laws have been tabulated. In their seminal study Boyer et al.¹² assume that the beads are frictional and explain the measured solid fraction value $\phi_J = 0.585$ at the jamming point by the existence of friction. Here we show that it is not the case at all. The measured solid fraction value is due to a swelling of the beads and the particles are frictionless. Accounting for a 1 μm swelled layer in the effective particle radius, leads to an effective jamming solid fraction $\phi_J^{\text{eff}} = 0.63$, as expected for frictionless particles.

PS beads in water exhibit electrostatic repulsive forces. In the studied suspension, in the range of shear stresses investigated, the interparticle force is lower than this repulsive force. This implies that there are no direct solid contacts between the particles, which leads to a frictionless behavior for the overall suspension. Consistently, we found a jamming solid

fraction of 0.63. When the interparticle force is larger than the repulsive force, particle contacts become frictional, with a friction coefficient that is equal to 0.1 (figure 10); the possible impact of the transition between lubricated and frictional contacts at a critical force could not be investigated within our system: it might be observed with larger PS beads.

This study on different solvents confirms a well-established idea among rheologists: very small variations in tangential and normal forces between particles profoundly affect rheological properties. Last but not least, we insist in the conclusion that it is the microscopic friction coefficient between particles that must be measured and not a macroscopic coefficient resulting from a measurement, where the ratio is made between an average normal force and a shear force applied on a layer of balls as in Tapia et al.²⁴. In the latter case, the experiment carried out does not consist in taking the average of the friction coefficient. The so-called normal force in these experiments, which is a macroscopic quantity, is not always normal to the various interparticle contacts at the microscopic scale, which distorts the friction coefficient measurement. We show in this study that the microscopic coefficient of the polystyrene particles in PEG is zero, whereas a macroscopic study on an assembly of similar beads concludes that it is 0.3.

Our study provides new quantitative data to test micromechanical models and simulations. It also paves the way to the fine tuning of the suspension rheology through the control of the material formulation and chemistry. Finally, it shows the need to systematically characterize the interparticle normal and tangential forces when studying a given suspension of hard spheres in a Newtonian fluid.

Acknowledgement

We acknowledge support from the Agence Nationale de la Recherche (project Fluididense ANR-17-CE07-0040) and the Institut Pierre-Gilles de Gennes (laboratoire d'excellence PSL, Investissements d'avenir program ANR-10-IDEX-0001-02 PSL and ANR-10-LABX-31 and ANR-10-EQPX-34).

References

- (1) Larson, R. G. *The structure and rheology of complex fluids*; Oxford university press New York, 1999; Vol. 150.
- (2) Guazzelli, É.; Pouliquen, O. Rheology of dense granular suspensions. *Journal of Fluid Mechanics* **2018**, *852*.
- (3) Papir, Y. S.; Krieger, I. M. Rheological studies on dispersions of uniform colloidal spheres: II. Dispersions in nonaqueous media. *Journal of Colloid and Interface Science* **1970**, *34*, 126–130.
- (4) Chatté, G.; Comtet, J.; Niguès, A.; Bocquet, L.; Siria, A.; Ducouret, G.; Lequeux, F.; Lenoir, N.; Ovarlez, G.; Colin, A. Shear thinning in non-Brownian suspensions. *Soft matter* **2018**, *14*, 879–893.

- (5) Arshad, M.; Maali, A.; Claudet, C.; Lobry, L.; Peters, F.; Lemaire, E. An experimental study on the role of inter-particle friction in the shear-thinning behavior of non-Brownian suspensions. *Soft Matter* **2021**,
- (6) Seto, R.; Mari, R.; Morris, J. F.; Denn, M. M. Discontinuous shear thickening of frictional hard-sphere suspensions. *Physical review letters* **2013**, *111*, 218301.
- (7) Wyart, M.; Cates, M. E. Discontinuous shear thickening without inertia in dense non-Brownian suspensions. *Physical review letters* **2014**, *112*, 098302.
- (8) Morris, J. F. Shear thickening of concentrated suspensions: Recent developments and relation to other phenomena. *Annual Review of Fluid Mechanics* **2020**, *52*, 121–144.
- (9) Leighton, D.; Acrivos, A. The shear-induced migration of particles in concentrated suspensions. *Journal of Fluid Mechanics* **1987**, *181*, 415–439.
- (10) Morris, J. F.; Boulay, F. Curvilinear flows of noncolloidal suspensions: The role of normal stresses. *Journal of rheology* **1999**, *43*, 1213–1237.
- (11) Rashedi, A.; Sarabian, M.; Firouznia, M.; Roberts, D.; Ovarlez, G.; Hormozi, S. Shear-induced migration and axial development of particles in channel flows of non-Brownian suspensions. *AIChE Journal* **2020**, *66*, e17100.
- (12) Boyer, F.; Guazzelli, É.; Pouliquen, O. Unifying suspension and granular rheology. *Physical review letters* **2011**, *107*, 188301.
- (13) Singh, A.; Mari, R.; Denn, M. M.; Morris, J. F. A constitutive model for simple shear of dense frictional suspensions. *Journal of Rheology* **2018**, *62*, 457–468.
- (14) Chèvremont, W.; Chareyre, B.; Bodiguel, H. Quantitative study of the rheology of frictional suspensions: Influence of friction coefficient in a large range of viscous numbers. *Physical Review Fluids* **2019**, *4*, 064302.
- (15) Lobry, L.; Lemaire, E.; Blanc, F.; Gallier, S.; Peters, F. Shear thinning in non-Brownian suspensions explained by variable friction between particles. *Journal of Fluid Mechanics* **2019**, *860*, 682–710.
- (16) Gálvez, L. O.; de Beer, S.; van der Meer, D.; Pons, A. Dramatic effect of fluid chemistry on cornstarch suspensions: Linking particle interactions to macroscopic rheology. *Physical Review E* **2017**, *95*, 030602.
- (17) Comtet, J.; Chatté, G.; Nigues, A.; Bocquet, L.; Siria, A.; Colin, A. Pairwise frictional profile between particles determines discontinuous shear thickening transition in non-colloidal suspensions. *Nature communications* **2017**, *8*, 1–7.
- (18) Madraki, Y.; Oakley, A.; Nguyen Le, A.; Colin, A.; Ovarlez, G.; Hormozi, S. Shear thickening in dense non-Brownian suspensions: Viscous to inertial transition. *Journal of Rheology* **2020**, *64*, 227–238.

- (19) Fall, A.; Lemaitre, A.; Bertrand, F.; Bonn, D.; Ovarlez, G. Shear thickening and migration in granular suspensions. *Physical review letters* **2010**, *105*, 268303.
- (20) Maranzano, B. J.; Wagner, N. J. The effects of particle size on reversible shear thickening of concentrated colloidal dispersions. *The Journal of chemical physics* **2001**, *114*, 10514–10527.
- (21) Lu, S.; Zhu, K.; Song, W.; Song, G.; Chen, D.; Hayat, T.; Alharbi, N. S.; Chen, C.; Sun, Y. Impact of water chemistry on surface charge and aggregation of polystyrene microspheres suspensions. *Science of the total environment* **2018**, *630*, 951–959.
- (22) Fall, A.; Ovarlez, G.; Hautemayou, D.; Mézière, C.; Roux, J.-N.; Chevoir, F. Dry granular flows: Rheological measurements of the μ (I)-rheology. *Journal of rheology* **2015**, *59*, 1065–1080.
- (23) Fall, A.; Bertrand, F.; Ovarlez, G.; Bonn, D. Yield stress and shear banding in granular suspensions. *Physical review letters* **2009**, *103*, 178301.
- (24) Tapia, F.; Pouliquen, O.; Guazzelli, É. Influence of surface roughness on the rheology of immersed and dry frictional spheres. *Physical Review Fluids* **2019**, *4*, 104302.